DNA Nanotechnology Hot Paper

DOI: 10.1002/anie.201403965

Surface-Assisted Large-Scale Ordering of DNA Origami Tiles**

*Ali Aghebat Rafat, Tobias Pirzer, Max B. Scheible, Anna Kostina, and Friedrich C. Simmel**

Abstract: *The arrangement of DNA-based nanostructures into extended higher order assemblies is an important step towards their utilization as functional molecular materials. We herein demonstrate that by electrostatically controlling the adhesion and mobility of DNA origami structures on mica surfaces by the simple addition of monovalent cations, large ordered 2D arrays of origami tiles can be generated. The lattices can be formed either by close-packing of symmetric, non-interacting DNA origami structures, or by utilizing blunt-end stacking interactions between the origami units. The resulting crystalline lattices can be readily utilized as templates for the ordered arrangement of proteins.*

In recent decades, self-assembly based on the specific and programmable recognition interactions between DNA molecules has been shown to be a successful strategy for the generation of artificial nanoscale molecular structures.[1] Most prominently, the DNA origami technique[2] has enabled the realization of almost arbitrarily shaped molecular objects, which can further be decorated with functional molecules or nanoparticles with a spatial resolution of only a few nanometers. This capability has already resulted in a variety of potential applications for DNA nanotechnology, ranging from nanomaterials[3] over biosensing[4] to nanomedicine.[5] For many applications, an extension of the "local order" facilitated by DNA self-assembly also to larger length scales would be desirable, for example, when the generation of macroscopic DNA-based materials is envisioned, or integration with top-down fabrication technologies is required.

Several features have been found to be useful for the generation of large-scale assemblies based on small (i.e., non-origami) DNA tiles. Apart from the development of rigid molecular building blocks,[6] sequence-symmetric interactions,[7] the precise control of nucleation and growth parameters,[8] and the utilization of weak, cooperative interactions have been shown to generate particularly well-ordered structures in two and even three dimensions.[9] Also the presence of a surface was found to promote the assembly of large ordered lattices from small T-junction units[10] or star-shaped tiles.[11]

DNA origami structures can adopt a larger diversity of shapes than small DNA tiles, and also allow for more complex chemical functionalization. Previous approaches toward the generation of larger DNA origami assemblies involved lithographic patterning,[12] the utilization of longer scaffold strands,[13] polymerization[14] and higher order assembly using hybridization[15] or blunt-end stacking interactions.[10,16] The only successful example of extended 2D crystallization of DNA origami tiles was demonstrated by Liu et al.[17] based on sticky-end hybridization of cross-shaped origami structures. Thermal annealing over several days resulted in crystalline 2D arrays with dimensions of up to $5 \times 10\ \mu m^2$.

We show herein that surface-assisted assembly[10,11] can also be achieved with DNA origami structures by simply improving their surface mobility by the addition of monovalent salts (Scheme 1). In typical atomic force microscopy (AFM) experiments on negatively charged mica sheets, DNA origami structures are strongly adsorbed to the substrate to facilitate stable imaging. Adsorption is mediated by Mg^{2+} ions (typically already contained in the origami folding buffer), which act as salt bridges between mica and DNA (Figure 1 A). This interaction can be weakened by the addition of monovalent ions, such as Na^+, which partly replace the Mg^{2+} ions and form a more diffuse charge layer between the surface and the polyelectrolyte.[18] As a result, the origami structures become mobile on the surface and can then associate to form extended ordered structures on the surface. We demonstrate that non-interacting, regularly shaped origami structures, such as rectangles[2a,19] or triangles,[2a] simply assemble into close-packed structures, dictated by the steric repulsion between the building blocks. In the case of twist-corrected, cross-shaped origami tiles[17] we also employ attractive blunt-end

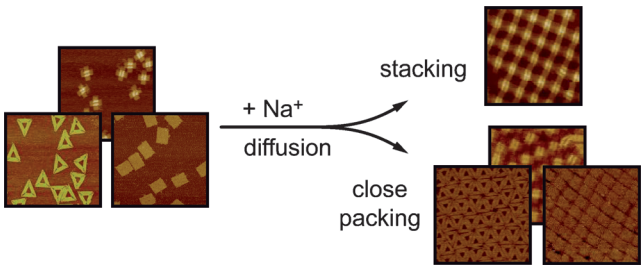

Scheme 1. The surface mobility of DNA origami structures on mica can be tuned by the addition of monovalent cations. Depending on the symmetry of the origami building blocks and their mutual interactions, large-scale ordered 2D assemblies can form.

[*] A. Aghebat Rafat,[+] Dr. T. Pirzer,[+] M. B. Scheible, A. Kostina, Prof. Dr. F. C. Simmel
Physik-Department E14 and ZNN/WSI, TU München
Am Coulombwall 4a, 85748 Garching (Germany)
E-mail: simmel@tum.de
Prof. Dr. F. C. Simmel
Nanosystems Initiative Munich
Schellingstrasse 4, 80539 Munich (Germany)

[+] These authors contributed equally to this work.

[**] We gratefully acknowledge financial support by the Volkswagen Stiftung (grant no. 86 395), the EU Marie Curie Initial Training Network EscoDNA, and the Cluster of Excellence Nanosystems Initiative Munich (NIM). We thank A. Kuzyk for initial work in this project.

Supporting information for this article is available on the WWW under http://dx.doi.org/10.1002/anie.201403965.

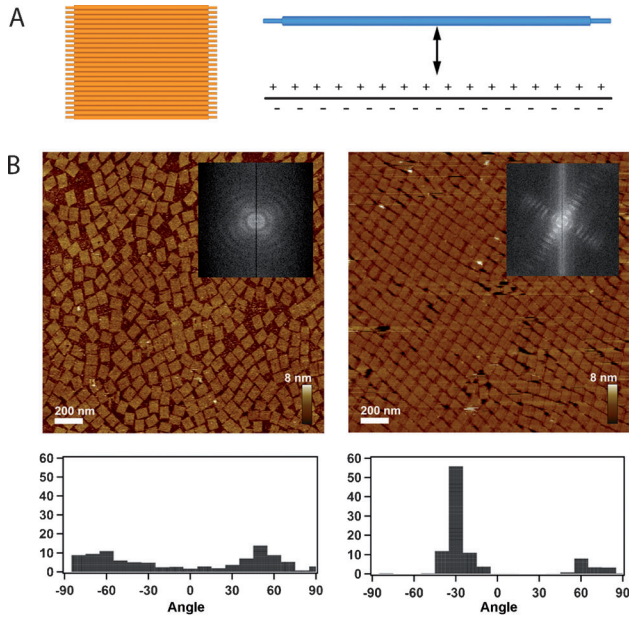

Figure 1. A) Left: representation of a regular rectangular DNA origami tile. Right: Schematic representation of an adsorbed origami structure (blue) on a negatively charged mica substrate (solid line). Cations are located between the tile and mica. Mg^{2+} ions act as salt bridges, whereas Na^{+} ions screen negative surface charge in a diffuse charge layer. B) AFM images of rectangular origami tiles on mica in the absence of NaCl (left) and in the presence of 200 mM NaCl (right) in the buffer solution. Insets: FFT images indicate the symmetry and the degree of order in the assemblies (see text). The histograms show the distribution of origami orientations with respect to the images' *y*-axes. The scan size of the images is 2 μm × 2 μm. The tile length of 100 nm and width of 80 nm were determined from the AFM images.

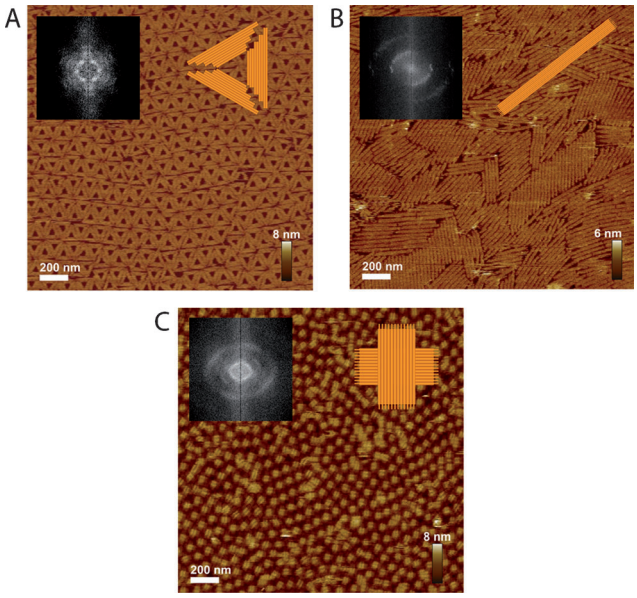

Figure 2. AFM images of origami assemblies made from A) triangles, B) long rectangles, and C) cross-shaped tiles. The symmetry of the base units determine the quality and degree of ordering as reflected in their FFT analyses (insets). Long-rectangular tile assembly is favored perpendicular to the long axis of a tile. Cross-shaped tiles show less ordering and rectangular symmetry. Blurred features in the FFT images indicate a distribution of the symmetry axes and the spatial frequencies of the base unit. The scan size is 2 μm × 2 μm. The measured dimensions of the tiles are 25 nm × 280 nm for the long rectangles, 126 nm per side for the triangles and 95 nm for the length of a cross-subtile.

stacking interactions, which combined with surface diffusion result in very large ordered origami cross lattices.

In Figure 1, surface-assisted assembly of rectangular origami tiles by close packing on mica is shown. In the presence of only Mg^{2+} ions, application of a solution of DNA origami rectangles to the mica substrate results in the adsorption of origami structures in only weakly correlated orientation (Figure 1 B, left). In contrast, a sample with added NaCl ([NaCl] = 200 mM) displays large-scale ordering with most origami structures aligned with the same orientation (Figure 1 B, right). To provide an objective measure for the symmetry and degree of ordering of the assemblies, we also performed fast Fourier transformation (FFT) analysis of the AFM images (cf. insets in Figure 1 B, 2 A–C). FFT maxima are found along the main spatial directions of the assemblies. Sharp FFT reflexes correspond to crystalline assembly, while blurred rings indicate amorphous structure. A larger number of discrete FFT spots also indicates a longer range of ordering. In the case of the close-packed rectangular origami tiles the rectangular symmetry of the lattice is clearly visible.

As indicated in Figure 2, diffusion-assisted close packing of origami structures also works well with other single-layered origami tiles, such as triangles,[2a] long rectangles,[19] or cross-shaped structures.[17] The degree of order that can be achieved in this way apparently depends on the symmetry of the base shape, its convexity, and also its "compactness" (or aspect ratio). Triangular origami tiles form a lattice with trigonal symmetry, which is clearly reflected in the FFT analysis. Compared to the rectangular tile lattice of Figure 1, there are less single-point defects (such as missing or broken tiles), but dislocations give the lattice a wavy structure, which reduces the degree of ordering in the FFT. Over a range of 1 μm and more, long-rectangular origami tiles (Figure 2 B) assemble very well in a direction perpendicular to their long sides, but do not display large-scale ordering in 2D. Even though the cross-shaped origami tiles could potentially tile the plane, they show an even lower degree of order, which results from diffusion traps created by their concave shape. An increase in $[Na^{+}]$ above 200 mM causes the close packed lattices to disintegrate. Close-packed tiles become more loosely packed and isolated origami tiles desorb from the substrate (see Supporting Information Figure S1).

To prevent disintegration of the origami superstructures at higher monovalent salt concentrations, we also employed stabilizing attractive interactions between the origami tiles. Strong interactions (e.g., by sticky-end hybridization) can however, result in fractal growth by a diffusion-limited aggregation mechanism.[20] For the growth of large crystalline areas from origami tiles, we thus employed weaker blunt-end stacking interactions[2a,16] that allowed reversible formation and breakage of bonds, and thus reorganization and healing of the growing crystals. As shown in Figure 3 A, we utilized a twist-corrected version of the cross-shaped origami tile

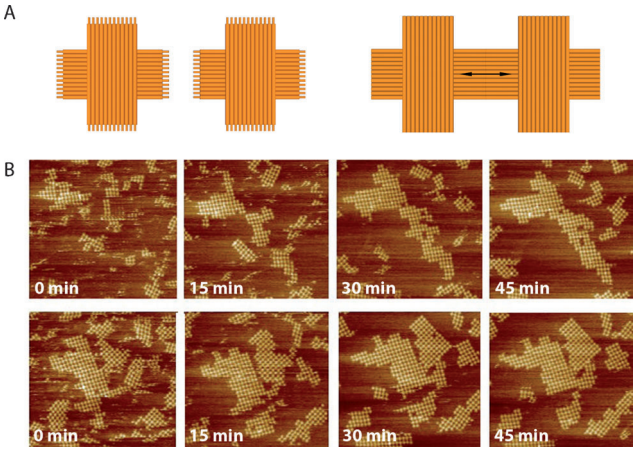

Figure 3. A) Left: Cross-shaped origami tiles without edge staples (single-stranded scaffold is orange) do not interact with each other. Right: Incorporation of edge staples creates blunt ends, which facilitate stacking interactions between the tiles. B) Two sets of AFM images of cross-shaped tiles with blunt ends on mica recorded during 2D crystallization, which progresses through a typical nucleation and growth process. [NaCl] = 420 mM. The scan size is 3 μm × 3 μm.

developed by Liu et al.[17] for 2D crystallization by blunt-end stacking.

Our experiments indicate that origami cross-tiles already oligomerize in solution (cf. Figure S2). Oligomers can adsorb on mica and then act as nuclei for 2D crystallization on the surface in a typical nucleation and growth process. Initially, the growing nuclei diffuse on the surface until stable immobile structures are formed. Single tiles or smaller assemblies still adsorb on the surface and start new nucleation sites, or fuse with larger assemblies.

In Figure 3B, we monitored the progress of 2D crystallization by AFM imaging at [NaCl] = 420 mM. A variety of processes can be identified that contribute to crystal growth: small distortions in the lattices heal and frayed edges are completed during the 2D assembly process. Point defects, such as single missing tiles, are filled up with monomers from bulk solution.

As can also be seen in Figure 3, the main limiting factor for unlimited crystal growth is the presence of disoriented immobile crystalline domains in close proximity to each other. Crystal formation was improved by rinsing a fully covered mica surface with pure water, which removes ions and all weakly bound assemblies from the surface (cf. Figure S3A,B). After drying and repeated overnight incubation in 1 × TAE containing 12.5 mM Mg_2Cl and 400 mM NaCl, larger crystalline domains with typical dimensions in the micrometer-range formed (Figure 4, cf. Figure S4 for FFT). Still many typical crystal-growth defects, such as point defects or dislocations are visible, which mainly occur at the boundaries between the domains. If the initial concentration of crystallization nuclei on the surface could be reduced further, potentially much larger lattices should be feasible. Low concentrations lead to smaller, less stable and more mobile clusters in the beginning, however, and thus the implementation of dedicated seed structures may be required.

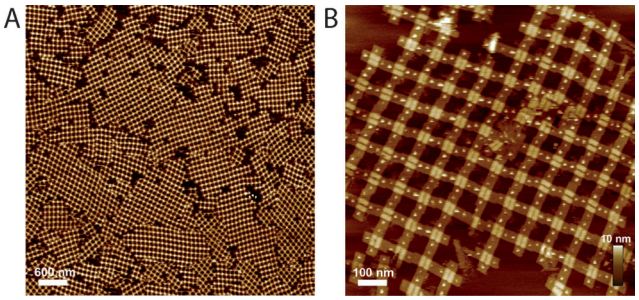

Figure 4. A) AFM image of 2D lattices made from cross-shaped DNA origami tiles. The central lattice domain has a length of about 6 μm and a width varying between 1 and 3 μm. B) AFM image of streptavidin bound to a 2D lattice of cross-shaped tiles equipped with biotin.

To demonstrate a potential application of our simple crystallization strategy, we utilized a cross-tile lattice for the ordered arrangement of proteins (Figure 4B, Figure S4B). To this end, each cross-shaped tile was functionalized with eight biotinylated staples, with two biotin moieties on each arm pointing above and below the plane defined by the cross. First a tile lattice was assembled on a mica surface, followed by decoration with streptavidin in situ. We found a high yield of 98% for occupation of the lattice positions. As the binding yield to a single biotin on an origami structure has been estimated to be approximately 86%,[21] this indicates that both biotin units (above and below the tile) are in fact available for binding. This may be explained by threading of the biotinylated staples through the origami as reported elsewhere.[22]

We note that in our assembly approach we currently cannot control the orientation of the tiles. In particular, neither the two sides nor the four arms of the origami cross-tiles are completely equivalent. Nevertheless, the cross tiles locally seem to associate in a preferred orientation, which can be identified from the origami substructure also visible in Figure 4B. Using a symmetric and redundant labeling with biotin as in Figure 4B, however, a streptavidin pattern can be generated that has a higher symmetry than the origami lattice itself.

We have demonstrated that by electrostatically controlling the mobility of DNA origami structures on a mica surface, large, ordered arrays of origami tiles can be easily generated. Inert origami tiles assemble into close-packed structures, while tiles interacting through blunt-end stacking form extended 2D crystals whose symmetry is dictated by the direction of the stacking "bonds". It should also be possible to implement a similar crystallization approach on other types of surfaces, which should be of interest for applications in nanomaterials. It is also conceivable to chemically cross-link the lattices after formation on mica and transfer them onto other substrates using soft lithographic methods. It may also be possible to grow origami-tile lattices along scaffold structures on the surface, and even to implement origami-based crystalline self-replication schemes.[23]

Experimental Section

Design and fabrication of the DNA nanostructures: DNA origami tiles were folded from a 7249 nucleotide (nt) long single-stranded DNA "scaffold" strand from the phage virus M13mp18 using short "staple" oligonucleotides (Eurofins MWG). Four different shape-variations were designed using caDNAno,[24] namely a twist-corrected rectangular tile, a long-rectangle, a triangle, and a cross-shaped tile, using 186, 186, 233, and 186 staple strands, respectively (cf. Supporting Figure S5 to S9). Staples were mixed with scaffold in 3.4-fold molar excess for triangular tiles and 1.4-fold molar excess (5.6-fold for edge staples) for other origami tiles in folding buffer (1 × TAE with 12.5 mM $MgCl_2$); for the streptavidin experiment 4.2-fold molar excess for edge staples and 4.5-fold molar excess for biotinylated staples were used. The mixture was heated to 70 °C and slowly annealed to room temperature (0.5 °C min^{-1} between 65–45 °C). To purify the folded origami structures, PEG precipitation was used.[25] Two equal volumes of sample solution and folding buffer (supplemented with 15 % PEG-8000 and 500 mM NaCl) were carefully mixed and centrifuged for 30 min at 4 °C (20000 rcf). The supernatant solution was slowly poured away, retaining the pellet, which was redissolved in PEG-buffer (repeating the process three times) and finally redissolved in the desired buffer solution.

Imaging of the DNA nanostructures: AFM imaging was performed on a Veeco Multimode V (with a Bruker Multimode 8 Controller) in intermittent contact mode under liquid conditions using silicon nitride cantilevers (SCANASYST-Fluid + from Bruker and BL-AC40TS-C2 from Olympus). Typical cantilever resonance frequencies were between 25–33 kHz and scan rates between 2–6 Hz. Images were post-processed by subtracting a 2nd-order polynomial from the image using the Nanoscope 8.15 software. To form crystalline structures, 40 μL of sample solution were deposited on freshly cleaved mica sheets for surface assisted 2D assembly. To weaken the attractive forces between structures and mica surface, the magnesium-containing folding buffer was supplemented with varying concentrations of sodium chloride ([NaCl] = 0.1–0.5 M), subsequently increasing the diffusion-driven mobility of origami structures enabling higher order crystal-like arrangements. The samples in Figure 4 A and Figure S3B were prepared as described in the main text.

Protein labeling: Cross-shaped tiles were modified with two biotinylated single-stranded extensions on each side arm, to which streptavidin proteins can bind. After the assembly and a waiting time of 1 hour the mica sample was washed in a petri dish containing folding buffer to purify the sample from unbound tiles. Afterwards the sample was incubated with 20 μL of 2 μM streptavidin solution and additional 30 μL of folding buffer for 90 min. Afterwards the mica sample was washed again in a petri dish and consecutively imaged in folding buffer.

Received: April 3, 2014
Published online: June 4, 2014

Keywords: DNA nanotechnology · DNA origami · self-assembly

[1] N. C. Seeman, *Annu. Rev. Biochem.* **2010**, *79*, 65 – 87.
[2] a) P. W. K. Rothemund, *Nature* **2006**, *440*, 297 – 302; b) S. M. Douglas, H. Dietz, T. Liedl, B. Högberg, F. Graf, W. M. Shih, *Nature* **2009**, *459*, 414 – 418.
[3] a) H. T. Maune, S.-p. Han, R. D. Barish, M. Bockrath, W. A. G. Iii, P. W. K. Rothemund, E. Winfree, *Nat. Nanotechnol.* **2010**, *5*, 61 – 66; b) P. K. Dutta, R. Varghese, J. Nangreave, S. Lin, H. Yan, Y. Liu, *J. Am. Chem. Soc.* **2011**, *133*, 11985 – 11993; c) A. Kuzyk, R. Schreiber, Z. Y. Fan, G. Pardatscher, E. M. Roller, A. Hogele, F. C. Simmel, A. O. Govorov, T. Liedl, *Nature* **2012**, *483*, 311 – 314.
[4] a) Y. G. Ke, S. Lindsay, Y. Chang, Y. Liu, H. Yan, *Science* **2008**, *319*, 180 – 183; b) B. Saccà, R. Meyer, M. Erkelenz, K. Kiko, A. Arndt, H. Schroeder, K. S. Rabe, C. M. Niemeyer, *Angew. Chem.* **2010**, *122*, 9568 – 9573; *Angew. Chem. Int. Ed.* **2010**, *49*, 9378 – 9383.
[5] a) V. J. Schüller, S. Heidegger, N. Sandholzer, P. C. Nickels, N. A. Suhartha, S. Endres, C. Bourquin, T. Liedl, *ACS Nano* **2011**, *5*, 9696 – 9702; b) A. S. Walsh, H. Yin, C. M. Erben, M. J. A. Wood, A. J. Turberfield, *ACS Nano* **2011**, *5*, 5427 – 5432; c) J. Li, H. Pei, B. Zhu, L. Liang, M. Wei, Y. He, N. Chen, D. Li, Q. Huang, C. Fan, *ACS Nano* **2011**, *5*, 8783 – 8789; d) S. M. Douglas, I. Bachelet, G. M. Church, *Science* **2012**, *335*, 831 – 834.
[6] a) E. Winfree, F. Liu, L. A. Wenzler, N. C. Seeman, *Nature* **1998**, *394*, 539 – 544; b) D. Liu, M. S. Wang, Z. X. Deng, R. Walulu, C. D. Mao, *J. Am. Chem. Soc.* **2004**, *126*, 2324 – 2325.
[7] Y. He, Y. Tian, Y. Chen, Z. Deng, A. E. Ribbe, C. Mao, *Angew. Chem.* **2005**, *117*, 6852 – 6854; *Angew. Chem. Int. Ed.* **2005**, *44*, 6694 – 6696.
[8] a) R. Schulman, E. Winfree, *Proc. Natl. Acad. Sci. USA* **2007**, *104*, 15236 – 15241; b) W. Li, Y. Yang, S. Jiang, H. Yan, Y. Liu, *J. Am. Chem. Soc.* **2014**, *136*, 3724 – 3727.
[9] a) M. Meng, C. Ahlborn, M. Bauer, O. Plietzsch, S. A. Soomro, A. Singh, T. Muller, W. Wenzel, S. Bräse, C. Richert, *ChemBioChem* **2009**, *10*, 1335 – 1339; b) J. Zheng, J. J. Birktoft, Y. Chen, T. Wang, R. Sha, P. E. Constantinou, S. L. Ginell, C. Mao, N. C. Seeman, *Nature* **2009**, *461*, 74 – 77.
[10] S. Hamada, S. Murata, *Angew. Chem.* **2009**, *121*, 6952 – 6955; *Angew. Chem. Int. Ed.* **2009**, *48*, 6820 – 6823.
[11] X. P. Sun, S. H. Ko, C. A. Zhang, A. E. Ribbe, C. D. Mao, *J. Am. Chem. Soc.* **2009**, *131*, 13248 – 13249.
[12] a) R. J. Kershner, L. D. Bozano, C. M. Micheel, A. M. Hung, A. R. Fornof, J. N. Cha, C. T. Rettner, M. Bersani, J. Frommer, P. W. K. Rothemund, G. M. Wallraff, *Nat. Nanotechnol.* **2009**, *4*, 557 – 561; b) A. E. Gerdon, S. S. Oh, K. Hsieh, Y. Ke, H. Yan, H. T. Soh, *Small* **2009**, *5*, 1942 – 1946.
[13] H. Zhang, J. Chao, D. Pan, H. Liu, Q. Huang, C. Fan, *Chem. Commun.* **2012**, *48*, 6405 – 6407.
[14] R. Jungmann, M. Scheible, A. Kuzyk, G. Pardatscher, C. E. Castro, F. C. Simmel, *Nanotechnology* **2011**, *22*, 275301.
[15] Z. Li, M. Liu, L. Wang, J. Nangreave, H. Yan, Y. Liu, *J. Am. Chem. Soc.* **2010**, *132*, 13545 – 13552.
[16] S. Woo, P. W. K. Rothemund, *Nat. Chem.* **2011**, *3*, 620 – 627.
[17] W. Liu, H. Zhong, R. Wang, N. C. Seeman, *Angew. Chem.* **2011**, *123*, 278 – 281; *Angew. Chem. Int. Ed.* **2011**, *50*, 264 – 267.
[18] D. Pastré, O. Pietrement, P. Fusil, F. Landousy, J. Jeusset, M. O. David, C. Hamon, E. Le Cam, A. Zozime, *Biophys. J.* **2003**, *85*, 2507 – 2518.
[19] R. Jungmann, C. Steinhauer, M. Scheible, A. Kuzyk, P. Tinnefeld, F. C. Simmel, *Nano Lett.* **2010**, *10*, 4756 – 4761.
[20] T. A. Witten, L. M. Sander, *Phys. Rev. Lett.* **1981**, *47*, 1400 – 1403.
[21] N. V. Voigt, T. Torring, A. Rotaru, M. F. Jacobsen, J. B. Ravnsbaek, R. Subramani, W. Mamdouh, J. Kjems, A. Mokhir, F. Besenbacher, K. V. Gothelf, *Nat. Nanotechnol.* **2010**, *5*, 200 – 203.
[22] N. Wu, D. M. Czajkowsky, J. J. Zhang, J. X. Qu, M. Ye, D. D. Zeng, X. F. Zhou, J. Hu, Z. F. Shao, B. Li, C. H. Fan, *J. Am. Chem. Soc.* **2013**, *135*, 12172 – 12175.
[23] a) R. Schulman, B. Yurke, E. Winfree, *Proc. Natl. Acad. Sci. USA* **2012**, *109*, 6405 – 6410; b) T. Wang, R. Sha, R. Dreyfus, M. E. Leunissen, C. Maass, D. J. Pine, P. M. Chaikin, N. C. Seeman, *Nature* **2011**, *478*, 225 – 228.
[24] S. M. Douglas, A. H. Marblestone, S. Teerapittayanon, A. Vazquez, G. M. Church, W. M. Shih, *Nucleic Acids Res.* **2009**, *37*, 5001 – 5006.
[25] S. M. Douglas, J. J. Chou, W. M. Shih, *Proc. Natl. Acad. Sci. USA* **2007**, *104*, 6644 – 6648.

